Choroid-resident macrophages maintain local vasculature and RPE integrity and spontaneously regenerate following depletion

Authors: Xiao Yang[1], Lian Zhao[1], Maria M. Campos[2], Mones Abu-Asab[2], Davide Ortolan[3], Nathan Hotaling[3], Kapil Bharti[3], and Wai T. Wong[*1]

Affiliations:

[1]Section on Neuron-Glia Interactions in Retinal Disease, National Eye Institute, National Institutes of Health, Bethesda, MD 20892, USA

[2]Section on Histopathology, National Eye Institute, National Institutes of Health, Bethesda, MD 20892, USA

[3]Section on Ocular and Stem Cell Translational Research, National Eye Institute, National Institutes of Health, Bethesda, MD 20892

*To whom correspondence should be addressed: Wai T. Wong, Section on Neuron-Glia Interactions in Retinal Disease, Building 6, Room 217, 6 Center Drive, National Eye Institute, National Institutes of Health, Bethesda, MD 20892, USA. Tel: +1 301 496 1758; fax: +1 301 496 1759; email: wongw@nei.nih.gov ORCID: 0000-0003-0681-4016

Author contributions:

Designed research (XY, LZ, WTW), contributed new reagents or analytic tools (MMC, MA-A, DO, NH, KB, WTW), analyzed data (XY, LZ, DO, WTW), wrote the paper (XY, LZ, MMC, MA-A, DO, NH, KB, WTW).

Significance Statement

Choroidal atrophy is associated with normal aging and progression in age-related macular degeneration (AMD), a leading cause of blindness. Herein, we identify the choroidal macrophage as a critical player in the homeostatic maintenance of choroid-RPE complex of the eye. Depletion of choroidal macrophages resulted in progressive vascular atrophy, altered structure of retinal pigment epithelial (RPE) cells, and dysregulated RPE expression of visual cycle protein and angiogenic factors, VEGF and PEDF. We discovered that choroidal macrophages can regenerate and repopulate the choroid following depletion, ameliorating RPE alterations and arresting vascular atrophy. Our results suggest that insufficiency of macrophage function may contribute to age- and AMD-associated pathology, and modulation of macrophage support functions may be therapeutically useful in AMD prevention and treatment.

Abstract:

The choroid of the eye provides necessary vascular supply to the outer retina across the retinal pigment epithelial (RPE) layer and is a locus of progressive degenerative change in aging and age-related macular degeneration (AMD). Cellular mechanisms that maintain or compromise choroidal vasculature homeostasis are not well understood, complicating therapeutic efforts. We discover here that pharmacological ablation of macrophages normally resident in the adult mouse choroid via blockade of the CSF1 receptor resulted in progressive thinning of the choroid layer and atrophy of the choriocapillaris. Concurrently, choroidal macrophage ablation also induced structural disorganization of the RPE cell layer, downregulation of RPE visual cycle genes, and altered RPE angiogenic factor expression. Suspension of CSF1R blockade following ablation conversely enabled spontaneous regeneration of the choroidal macrophage population, restoring original macrophage distribution and morphological features. Macrophage repopulation significantly ameliorated the ablation-induced changes in RPE structure and angiogenic factor expression and arrested choroidal vascular atrophy. These findings reveal a previously unsuspected trophic function of resident choroidal macrophages in the maintenance of choroidal vasculature and the RPE layer, suggesting that insufficiency of macrophage function may contribute to age- and AMD-associated pathology. Modulating choroidal macrophage support function can constitute a strategy for therapeutic preservation of the choroid and RPE in AMD prevention and treatment.

Introduction

The choroid of the mammalian eye comprises a dense vascular network located external to the retina and provides necessary material transport to the outer retina across the retinal pigment epithelial (RPE) layer constituting the outer blood retinal barrier (1). The functional significance of the choroidal supply is underscored by the implication of choroidal vascular atrophy as a significant contributor to degenerative diseases of the outer retina, particularly age-related macular degeneration (AMD)(2, 3), a current leading cause of blindness in the developed world (4). While progressive loss of choroidal vasculature has been observed with aging and AMD (5, 6), the mechanisms that either actively drive choroidal atrophy or fail to sustain choroidal homeostasis are not well understood, and treatments that can successfully preserve choroidal structure are unavailable.

Like in vascular networks located at border regions surrounding the brain within the dura mater, subdural meninges and choroid plexus (7, 8), the choroid of the eye contains a large constituent population of innate immune cells in the form of resident choroidal macrophages (9, 10). Under normal conditions, these macrophages are distributed across the entire choroid in the perivascular space in close juxtaposition with choroidal vessels. As they possess ramified cellular processes that demonstrate dynamic behavior, choroidal macrophages can potentially survey the perivascular environment and exchange signals with nearby vascular and RPE cells (11). While activated choroidal macrophages have been implicated in contributing to pathological changes in posterior uveitis (12) and choroidal neovascularization (13), their endogenous functions under healthy conditions are obscure, and if and how they may contribute to homeostasis in the choroid are not understood.

Dysfunction in choroidal macrophages has been linked to choroidal vascular alterations detected in aging and in AMD. Altered macrophage morphology and distribution have been correlated with attenuation of the choriocapillaris in the aged mouse choroid (11), and increased density and expression of activation markers in macrophages have been documented with the onset of AMD in human eyes (14), suggesting a causal relationship between macrophage changes and vascular loss. The implication of choroidal vascular loss as a driver of drusen accumulation and RPE disruption in AMD pathogenesis (15-17) have prompted strategies aimed at maintaining choroidal vascular health and improving vascular supply to the outer retina (18, 19), but the intrinsic mechanisms that maintain vascular and RPE integrity in the choroid have not been elucidated, limiting translational efforts.

We investigated here the contributions choroidal macrophages make to the homeostatic maintenance of choroidal vasculature and RPE cells by ablating of resident choroidal macrophages in a sustained manner. We examined the consequence of macrophage ablation using *in vivo* structural imaging and histopathological and molecular analyses. We discover that with depletion of choroidal macrophages, progressive vascular atrophy results, and was accompanied by multiple structural and functional changes in the RPE layer, resembling those observed with aging and AMD. We also discovered that residual choroidal macrophages following depletion can undergo regeneration. Although normally non-proliferative in nature, residual macrophages following depletion proliferated *in situ* and underwent morphological maturation to fully reconstitute features of the endogenous macrophage population. These regenerated macrophages restored endogenous macrophage homeostatic functions, as evidenced by their ability to arrest vascular atrophy and ameliorate RPE alterations upon repopulation of the choroid.

Our findings uncover a previously unsuspected constitutive function for resident choroidal macrophages in maintaining structural and functional homeostasis of choroidal vasculature and RPE cells and the ability of macrophages to regenerate the full complement of cells following depletion. These suggest a potential etiological mechanism of macrophage insufficiency for pathological choroidal vascular atrophy and highlight choroidal macrophage renewal as a phenomenon that may be potentially harnessed in regenerative strategies in the outer retina. Modulating choroidal macrophage presence and phenotype may be therapeutically effective in maintaining choroidal vasculature and consequently delaying AMD progression.

MATERIALS AND METHODS

Experimental animals

Experiments were conducted according to protocols approved by the National Eye Institute Animal Care and Use Committee and adhered to the Association for Research in Vision and Ophthalmology statement for the use of animals in ophthalmic and vision research. Animals were housed in a National Institutes of Health (NIH) animal facility under a 12-hour light/12-hour dark cycle with food *ad libitum*. Adult 3 month-old wild type BALB/cJ mice (The Jackson Laboratory, Bar Harbor, ME) and albino transgenic mice, containing a transgene with a α-smooth muscle actin (αSMA) promoter driving the expression of green fluorescent protein in perivascular cells in the choroid (20), were used to analyze cellular changes in the choroid and the RPE following macrophage depletion.

Model for macrophage depletion-repopulation in the choroid

We employed a model for macrophage depletion in the adult mouse choroid which involved the dietary administration of PLX5622 (Plexxikon, Berkeley, CA), a potent and selective inhibitor of the CSF1R that we previously demonstrated to deplete microglia in the retina (21). Animals were placed on a rodent chow containing PLX5622 (at 1200 parts per million, formulated by Research Diets Inc. New Brunswick, NJ) for up to 7 weeks to induce depletion macrophages resident in the choroid. To allow for the repopulation of choroidal macrophages, animals subjected to depletion with PLX5622-containing diet for 3 weeks were switched back to a standard diet; the first day of control diet resumption was designated day 0 of the repopulation phase.

Immunohistochemical analysis of sclerochoroidal tissue

Mice were euthanized by CO_2 inhalation. Enucleated eyes were dissected to form posterior segment eyecups which were then fixed in 4% paraformaldehyde in PBS for 1 hour at room temperature. Eyecups were dissected to obtain sclerochoroidal flatmounts, which were then immersed for 1 hour in a blocking buffer (1×PBS containing 10% normal goat serum and 0.5% Triton X-100) at room temperature. Primary antibodies, which included IBA1 (1:200; Wako), MHC-II (1:200; BD Pharmingen), or RPE65 (1:200; Millipore), were diluted in blocking buffer and added to flatmounts to incubate for 24 hours at 4°C. After washing in 1×PBS with 0.2% Triton X-100, sections were then incubated overnight with secondary antibodies (Alexa Fluor 488– or 568–conjugated anti-rabbit, rat or mouse IgG). Phalloidin (1:500; Invitrogen) was added and incubated for 4 hours label F-actin that enables visualization of RPE cell morphology. DAPI (1:500; Sigma-Aldrich) was added to label cell nuclei. Stained sclerochoroidal flatmounts were imaged with confocal microscopy (Zeiss LSM700). To visualize macrophage distributions over the entire choroid, tiled images of sclerochoroidal flatmounts were obtained under a 10x objective and stitched together with image analysis software (Zen, Carl Zeiss Microscopy). For visualization of RPE monolayer, multiplane z-series were captured under a 40x oil-immersion objective. Resulting images were subjected to computer-assisted analysis (ImageJ, NIH); the density of choroidal macrophages was assessed across the entire choroid and expressed as number per unit area. The number of nuclei per RPE cells were manually assessed from high-magnification images of RPE flat-mounts captured at or near the midpoint between the optic nerve and the peripheral edge of the flat-mount.

Automated RPE Morphological Analysis

Sclerochoroidal flatmounts immunolabeled with RPE65 and phalloidin were imaged with confocal microscopy (Zeiss LSM880) and multiplane z-series images were captured under a 40x oil-immersion objective. Morphological analyses of RPE mosaics were performed in an automated manner using REShAPE software, as previously described (22). Briefly, individual RPE cells were segmented at their

borders using MATLAB and a binary "mask" has been generated to measure cell morphological features. RPE cell density was calculated as cell numbers per unit area and the area of individual RPE cells was determined from cell segmentation.

***In vivo* optical coherence tomography (OCT) imaging of the choroid**

Mice were anesthetized with intraperitoneal ketamine (90 mg/kg) and xylazine (8 mg/kg) and their pupils were dilated. Choroidal and retinal structure was assessed using OCT imaging (Spectralis, Heidelberg Engineering) in anesthetized animals through a dilated pupil. OCT images in the enhanced depth imaging (EDI)-mode were captured longitudinally in individual experimental animals in the same matched fundus location (with images captured using "follow-up" mode in the instrument software). The imaging was performed using a 30x objective (Heidelberg) and scan fields, measuring 6.5 by 4.4 mm and centered on the optic nerve (1000 A-scans/horizontal B-scan, 25 horizontal B-scans, average of three frames per B-scan, each spaced 182 µm apart) were captured in each imaging session. Repeat OCT imaging was performed at 1, 3, 5, and 7 weeks following the initiation of PLX5622. Thickness measurements in OCT images were made using the instrument manufacturer software; choroidal thickness measurements (defined as the axial distance from the Bruch's membrane to the outer edge of the choroid) were measured at 300 µm temporal and nasal from the optic nerve on the horizontal meridian, and average retinal thickness measurements per eye (defined as the axial distance from the vitreal surface to the Bruch's membrane) were made at 300 µm temporal and nasal from the optic nerve in corresponding locations.

Direct labeling and visualization of choroidal vessels

Choroidal vessels are labeled by cardiac perfusion of an aqueous solution containing 1,19-dioctadecyl-3,3,39,39-tetramethylindocarbocyanine perchlorate (DiI, D-282, Invitrogen/Molecular Probes, Carlsbad, CA), a lipophilic dye that incorporates into membranes of endothelial cells revealing the structure of choroidal vessels as previously described (11). Briefly, experimental mice were euthanized by carbon dioxide inhalation and the thoracic cavity opened to expose the heart. A volume of 100 µL of DiI stock solution (6 mg/ml in 100% ethanol) was dissolved in 5 ml of diluent comprising 1xPBS and 5% glucose in a 1:4 ratio and the resulting solution delivered via cardiac perfusion at a rate of 1–2 mL/min. This was immediately followed by the perfusion of 6 mL of PBS. The animals were immediately enucleated and the retinal pigment epithelium (RPE)-sclera-choroid complex dissected from the harvested globes after fixation with 4% paraformaldehyde. These flat-mount preparations were mounted on glass slides in Fluoromount (Sigma-Aldrich) with the RPE cell layer uppermost. Confocal multiplane z-stack images of DiI-labeled endothelial cells were obtained with confocal microscopy (Zeiss LSM700) under a 63x oil-immersion objective. Images of labeled vessels in the choriocapillaris were used to compute the fraction of vascular coverage as the fractional area of the imaging field occupied by DiI-labeled vessels using ImageJ Software (NIH).

Quantitative reverse transcription PCR analysis

Quantitative reverse transcription-PCR analysis of isolated mouse choroid was performed to identify the molecular changes after macrophage depletion. RPE-sclerochoroidal tissue were acutely isolated from euthanized animals and total RNA was extracted using a RNeasy Mini kit (Qiagen) and amplified to cDNA using the PrimeScript 1st strand cDNA synthesis kit (TaKaRa Bio) per manufacturers' instructions. cDNA in 1 µL volume was used for real-time PCR analysis using SYBR Green PCR Mastermix (Affymetrix) on the CFX96 Real-Time System (Bio-Rad). Levels of mRNA expression were normalized to those in controls as determined using the comparative CT ($2\Delta\Delta CT$) method. GAPDH was used as an internal control. Tgfb1 primer was purchased from Bio-Rad (Assay ID qMmuCID0017320), and other oligonucleotide primer pairs used are listed in Supplementary Table 1.

Histological Analysis of Choroid-RPE Sections

Eyes from control and 7 weeks PLX5622-treated animals were isolated and fixed for 30 min in 4% glutaraldehyde followed by 10% formalin for at least 24 hours. Fixed eyes were embedded in methacrylate, serially sectioned and stained with hematoxylin and eosin. Images were taken with a Zeiss microscope and mean thickness of the choroid from temporal and nasal quadrants and mean cross-sectional area of vascular lumina were measured using ImageJ software (NIH).

Transmission Electron Microscopy of RPE Sections

The eyes from control and PLX5622-treated mice were isolated and fixed in 2.5% glutaraldehyde. The specimens were prepared for transmission electron microscopy (TEM) as previously described (23). Briefly, specimens were embedded in Spurr's epoxy resin and processed into ultrathin sections (90 nm) which were then stained with uranyl acetate and lead citrate and imaged with a transmission electron microscope (JEOL, JM-1010).

Protein quantitation in choroid-RPE-complex

Mouse RPE-choroidal samples were isolated from the following groups: untreated control group, group treated with 7 weeks of PLX5622, group treated with 3 weeks of PLX5622 and switched to regular diet for another 4 weeks to allow macrophage repopulation. Four biological replicates were obtained for each group. Pigment epithelium-derived factor (PEDF) protein levels were measured in the samples using the Mouse SERPINF1/PEDF ELISA kit (LifeSpan BioSciences; LS-F36110). Protein levels of VEGF, PDGF-AA and PDGF-BB were analyzed using a Magnetic Luminex Assay kit (R&D Systems, LXSAMSM-11).

Electroretinographic (ERG) analysis

ERGs were recorded using an Espion E2 system (Diagnosys). Mice were dark-adapted for 12 h and their pupils were dilated prior to ERG assessment. Mice were anesthetized and flash ERG recordings were obtained simultaneously from both eyes using gold wire loop electrodes, with the reference electrode placed in the animal's mouth and the ground subdermal electrode at the tail. ERG responses were obtained at increasing light intensities over the ranges of 1×10^{-4} to 10 cd·s/m^2 under dark-adapted conditions, and 0.3 to 100 cd·s/m^2 under a background light that saturates rod function. The stimulus interval between flashes varied from 5s at the lowest stimulus strengths to 60 s at the highest ones. Two to ten responses were averaged depending on flash intensity. ERG signals were sampled at 1 kHz and recorded with 0.3 Hz low-frequency and 300 Hz high-frequency cutoffs. Analysis of a-wave and b-wave amplitudes was performed using customized Espion ERG Data Analyzer software (v2.2) that digitally filters out high-frequency oscillatory potential wavelets. The a-wave amplitude was measured from the baseline to the negative peak and the b-wave was measured from the a-wave trough to the maximum positive peak. ERGs were recorded before and after macrophage depletion. The a- and b-wave measurements of animals with or without macrophage depletion were compared using a two-way ANOVA.

Statistical analysis

Statistical analyses were performed using Prism 7.0d (GraphPad). For comparisons involving two data columns, t tests (paired or unpaired) or nonparametric tests (Mann–Whitney U) were used, depending on whether the data followed a Gaussian distribution as determined by normality tests. A normality test (D'Agostino and Pearson) was used to analyze the distribution of all datasets. For comparisons involving three or more data columns, a one-way ANOVA (with Dunnett's multiple-comparisons test) was used if the data in an experimental group were found in a Gaussian distribution, and a nonparametric Kruskal–Wallis test (with Dunn's multiple-comparisons test) was used otherwise.

RESULTS

Sustained depletion of resident macrophages in the choroid induces progressive choroidal thinning and vascular atrophy

To investigate the endogenous contribution of resident macrophages to the structure of the adult mouse choroid, young (3-month old) adult wild type BALB/cJ mice were administered a diet containing PLX5622, an inhibitor of the macrophage-expressed receptor CSF1R, which regulates macrophage survival (24). Compared with the choroid of control animals fed a regular diet, which had a typical network of ramified MHCII+ and IBA1+ resident macrophages (9, 11), those in PLX5622-administered animals demonstrated a widespread depletion of macrophages in all topographical areas of the choroid, with a small number of residual MHCII+, IBA1+ cells showing a non-ramified morphology (Fig. 1A). Following 1 week of PLX5622 administration, the density of MHCII+, IBA1+ macrophage decreased to ≈10% of that in control animals and was sustained at these levels with continuous PLX5622 administration for up to 7 weeks (Fig. 1B). Expression of *Iba1* mRNA in sclerochoroidal tissue was correspondingly decreased from baseline levels at week 1 and week 7 of PLX5622 administration (Fig. 1C), indicating that CSF1R inhibition resulted in a rapid and comprehensive depletion of resident myeloid cells from the choroid.

As macrophage depletion has been causally associated with vascular changes in pathological contexts in the retina (25) and elsewhere (26), but is of lesser consequence to normal adult retinal vasculature (27), we investigated whether choroidal macrophages exert a trophic influence in the healthy adult vascular choroid by examining the effects of macrophage depletion. *In vivo* enhanced-depth OCT images captured in a longitudinal manner before and during PLX5622 administration revealed significant and progressive reductions in choroidal thickness across the entire area of the choroid; measurements made in both the nasal and temporal quadrants showed time-dependent decreases with sustained PLX5622 administration, declining to ≈70% of baseline values by 7 weeks (Fig. 2A, B). By contrast, the structure of the laminated retina and total retinal thickness measurements in the same experimental animals were unchanged during PLX5622 administration (Fig. 2C).

Histological analyses of choroidal vascular structure in stained retinochoroidal cryosections demonstrated corresponding significant decreases in the mean thickness of the vascular layer of the choroid (Fig. 2D, E). Quantitative analysis of vascular lumina in cryosections found reductions in the mean cross-sectional area of vascular lumina and the mean density of choroidal vessels (Fig. 2F). Quantitative analysis of choriocapillaris structure in sclerochoroidal flatmounts of DiI-perfused animals showed decreased vascular area coverage by choriocapillaris vessels (Fig. 2G, H). Together these findings demonstrate that sustained depletion of choroidal macrophages induced generalized vascular atrophy in the adult mouse choroid, a feature not observed in the adult retina. These vascular changes were not associated with a marked loss and disorganization of the population of smooth muscle actin (SMA)-expressing choroidal perivascular cells in the choroid (20), as evidenced by their maintained organization and morphology in macrophage-depleted animals (Fig. S1A, B).

Sustained depletion of choroidal macrophages induces aberrant RPE structure, gene expression, and function

As choroidal macrophages have been implicated in influencing RPE physiology in the context of macrophage-RPE-vascular interactions (28, 29), we investigated whether macrophage depletion from

the healthy adult choroid exerted influences on the overlying RPE layer. Following 7 weeks of PLX5622 administration, immunohistochemical analysis of the RPE layer showed decreased immunopositivity of RPE65, a constitutively expressed, RPE-specific enzyme that is required to maintain visual cycle function (30). Immunopositivity for RPE65, which was prominent and uniform in control animals, was decreased in depleted animals in a patchy, heterogenous manner, with a reduction in overall expression (Fig. 3A, B). These changes corresponded to a decrease in *Rpe65* mRNA expression (Fig. S2A), as well as in significantly decreased mRNA expression of genes mediating visual cycle function (*Lrat, Cralbp, Rlbp1*), RPE differentiation (*Mitf*), and tight junction structure (*Tjp1/Zo1*) (Fig. S2A-C). Electron microscopic analysis of RPE cell structure showed disrupted apical microvilli structure and increased vacuolation in depleted animals relative to control animals (Fig. 3C). In depleted animals, increased irregularity in the cell areas of individual RPE cells was noted on F-actin labeling; the mean overall RPE cell density was significantly decreased, corresponding to an increased proportion of enlarged cells (cell area > 900μm^2) (Fig. 3D). Enlarged cells in depleted animals showed an abnormal increase in cellular nuclei (usually 3-4 nuclei), a feature not observed in control animals (Fig. 3E). While the proportions of mono- and binucleated cells which constituted the majority of RPE cells were unchanged with depletion, RPE cells demonstrated a generally increased intracellular vacuolation on light microscopy. These changes in RPE morphology and expression of genes mediating RPE function were associated with concurrent reductions in electroretinographic responses in the form of decreased scotopic a- and b-wave amplitudes (Fig. 3F). Together, these data indicate that resident choroidal macrophages constitutively maintain aspects of RPE organization and gene expression that are important for RPE function in the healthy adult animal.

Angiogenic factor expression in the RPE-choroid complex is altered with choroidal macrophage depletion

As vascular structure of the adult choroid requires constitutive trophic support provided by angiogenic factors, in particular vascular endothelial growth factor (VEGF), for homeostatic maintenance (31, 32), we investigated whether choroidal macrophage depletion influences endogenous angiogenic factor expression in the RPE-choroid complex. We found that mRNA levels of *Vegfa* and *Vegfc* (Fig. 4A) and protein levels of VEGF (Fig. 4B) were significantly reduced in the RPE-choroid complex following 7 weeks of macrophage depletion. Consistent with this, we observed that immunopositivity for VEGF in cross-sections of the RPE-choroid complex, which is detected predominantly in the RPE layer in control animals, was decreased following macrophage depletion (Fig. 4C). We also analyzed the expression of pigment epithelium-derived factor (PEDF), a secreted, multi-functional anti-angiogenic agent capable of suppressing choroidal neovascularization (33, 34). We found that *Pedf* mRNA and PEDF protein levels (Fig. 4D, E), as well as PEDF immunopositivity in the RPE layer, were all significantly increased following macrophage depletion (Fig. 4F). In contrast, mRNA and protein expression levels of platelet-derived growth factor (PDGF) ligands, PDGF-AA and PDGF-BB, factors implicated in pericyte recruitment and vascular stabilization in the retina (35), were not markedly altered by macrophage depletion (Fig. 4G,H). These data suggest that altered expression of trophic factors generally, and a decrease in the ratio of VEGF/PEDF secretion specifically (36), occurs in the RPE-choroid as a consequence of macrophage depletion, and may constitute a mechanism contributing to the choroidal vascular atrophy observed.

Past studies had indicated that RPE-derived VEGF are required for vascular survival in the choroid (32, 37), and that TGF-β1 can induce VEGF expression in the RPE cells (38). We found that *Tgfb1* mRNA levels and TGFB1 immunopositivity were reduced in the choroid following 7 weeks of macrophage depletion

(Fig. S3A, B). Taken together, these data suggested that changes in angiogenic factor expression may underlie macrophage-mediated vascular support.

Macrophages in the choroid demonstrate spontaneous regeneration to repopulate the choroid following depletion

We and others have previously demonstrated that microglia normally resident in the adult retina can demonstrate spontaneous repopulation following depletion (21, 39). However, whether choroidal macrophages in the adult choroid can regenerate is unknown. To investigate this, we depleted choroidal macrophages in young adult mice for 3 weeks using a PLX5622-containing diet (depletion phase), and then reverted these animals to a standard diet for another 4 weeks (repopulation phase) (Fig. 5A). An age-matched group fed a standard diet served as a control. We observed that when macrophage-depleted animals were returned to a standard diet, MHCII+, IBA1+ macrophages rapidly reappeared in the choroid, with cell density reaching 50% of control levels after 1 week of repopulation, attaining 100% of control levels at 4 weeks, and remaining stable at that level thereafter (Fig. 5B, C). This increase in macrophage cell numbers was at least in part enabled by local proliferation of residual IBA1+ cells; while resident macrophages in the choroid of control animals were mostly non-proliferative and negative for the proliferation marker Ki67, prominent numbers of Ki67+,IBA1+ cells were detected at 1 week of repopulation when macrophage numbers were rising sharply (Fig. S4A, B). At 4 weeks repopulation, Ki67+ cell counts decreased back to control levels at a time when macrophage numbers have recovered to control levels. These observations reveal a previously uncharacterized regenerative capability of choroidal macrophages in which local proliferation of myeloid cells in the choroid contributes to the recovery of the macrophage population following depletion.

During the repopulation process, choroidal macrophages demonstrated features of phenotypic maturation *in situ*. Although all choroidal macrophages in the control animals showed immunopositivity for both MHCII and IBA1, we observed that a fraction of IBA1+ macrophages at 1 week in the repopulation phase were MHCII-negative, while no MHCII+ macrophages were IBA1-negative (Fig. 5D). This fraction of MHCII-, IBA1+ macrophages diminished with time and was undetectable at 6 weeks of repopulation, indicating MHCII as a later marker acquired by repopulating macrophage during maturation *in situ*. Repopulating macrophages also demonstrate maturation in terms of their morphological features. At 1 week of repopulation, although IBA1+ cell numbers had risen substantially to about 50% of control levels, most macrophages showed a deramified morphology with only a few short rudimentary processes. From 2 to 6 weeks of repopulation, macrophages developed progressively increased ramification, increasing in cell area, number of cellular processes, and dendritic field area, to acquire morphological features that were similar from choroidal macrophages in control animals (Fig. S4C-F).

Recovery of macrophages via regeneration arrests depletion-related degenerative changes in the RPE-choroid complex

To investigate the functional implications of choroidal macrophage regeneration following depletion, we evaluated the effect of repopulating macrophages on the structure of the RPE-choroid complex. We compared (1) animals that were subjected to macrophage depletion for 3 weeks and then allowed to repopulate for another 4 weeks (the depletion/repopulation group) with (2) animals subjected to continuous depletion for a total of 7 weeks (the continuous depletion group) (Fig. 6A). We found on OCT imaging that while choroidal thicknesses in the continuous depletion group declined progressively

over 7 weeks, those in the depletion-repopulation group stabilized upon the initiation of macrophage repopulation, and were significantly higher than those in the continuous depletion group at the end of the 7-week experiment (Fig. 6B). Assessment of choriocapillaris structure in choroidal flatmounts also found that areal coverage by choriocapillaris vessels decreased progressively over 7 weeks in the continuous depletion group, those in the depletion-repopulation group stabilized between 3 to 7 weeks during macrophage repopulation (Fig. 6C). These findings indicate that repopulating macrophages were able to functionally support the vascular structure of the choroid and provide further evidence for the constitutive contribution of choroidal macrophages to vascular maintenance.

We similarly assessed the function of repopulating macrophages in the support of RPE layer in these two experimental groups (Fig. 7A). In the continuous depletion group, mean RPE density at 3 weeks of depletion were similar to untreated controls but decreased at 7 weeks of depletion; in the depletion-repopulation group, mean RPE density was largely unchanged across 7 weeks (Fig. 7B). Analysis of the distribution of individual RPE cell areas showed that while RPE cells in continuously depleted animals showed a corresponding shift towards an increased prevalence of larger cells at 7 weeks depletion, those in the depletion-repopulation group were similar to those in untreated controls (Fig.7C). Further, macrophage repopulation also prevented the increase of multinucleated cells (≥ 3 nuclei) induced with 7 weeks depletion (Fig. 7D). These findings indicated that structural changes in RPE cells, a phenotype of later onset apparent at 7 weeks but not at 3 weeks of depletion, can be prevented if the choroidal macrophage population were reinstated by repopulation.

The effects of macrophage repopulation on RPE structure were also observed in analyses of RPE gene expression. Relative to the continuous depletion group, the depletion repopulation group showed amelioration in depletion-induced decreases in mRNA (Fig. S5A) and protein (Fig. 7E) expression of RPE65, and mRNA expression of visual cycle genes (*Lrat* and *Rlbp1*), *Mitf*, and *Tjp1/Zo1* (Fig. S5A-C). Depletion-induced reductions in *Vegfa* and *Vegfc* mRNA and VEGF protein expression were largely reversed with repopulation (Fig. 8A), while there was a trend towards a reversal of depletion-induced increases of *Pedf* mRNA and PEDF protein expression (Fig. 8B). Taken together, these data demonstrate that structural and gene expression changes induced in the RPE-choroid complex following macrophage depletion can be significantly ameliorated with macrophage repopulation, supporting the notion of a homeostatic supportive function for choroidal macrophages.

DISCUSSION

Tissue-resident innate immune cells, in addition to playing multiple inflammation-related functional roles, are now recognized to carry out constitutive homeostatic functions in adult tissues (40). In the adult brain, these cell populations comprise of microglia, which are located behind the blood-brain barrier (BBB) within the brain parenchyma (41), and border-associated macrophages, which are located external and adjacent to the BBB in the meninges and choroid plexus (7). How these populations mediate CNS homeostasis under normal conditions is an active area of investigation (42). In the eye, microglia resident within the healthy retina help maintain the structural and functional integrity of neuronal synapses (27), but the role of resident macrophages within the choroid of the eye is less well understood (43). Significantly, deficiencies in maintaining long-term structural homeostasis of the choroid feature importantly in ocular pathologies; the vascular choroid in in clinical studies has been found to undergo progressive atrophic thinning with normal aging (44-46) and with increasing severity of AMD (5), which are supported by histopathological and molecular evidence of vascular dropout and attenuation in these scenarios (3, 47-49). Previous studies have associated AMD severity with increased choroidal macrophage number and activation (14), however whether age-related and AMD-related choroidal changes may arise from deficient homeostatic function of resident macrophages has not been previously addressed.

In the current work, we discover that resident macrophages in the choroid play a previously unsuspected trophic role in maintenance of the vascular structure of the choroid. We found that the depletion of a significant majority of choroidal macrophages induced a generalized and progressive atrophy of the choroidal vasculature affecting choroidal vessels at multiple levels. This atrophic process extended to multiple levels of the vascular choroid, resulting in an overall decrease in choroidal thickness and choriocapillaris attenuation at the border of the RPE-Bruch's membrane interface. The ability of resident innate immune cells to maintain local vasculature appears to vary according to tissue context; within the CNS, the depletion of retinal or brain microglia results induces changes in vessel structure and permeability in developing systems (50, 51), but not in adult systems (27, 52). In the adult gut, the depletion of resident macrophage subsets results in vascular alterations in the submucosa (53), a feature observed analogously in the adult choroid. Resident macrophages in the choroid are distributed in a manner suitable for vascular regulation; they are found in close proximity to choroidal vessels at all levels and possess a dendritiform ramified morphology with dynamic cellular processes that constitutively survey the perivascular space (9, 11). As such, choroidal macrophages may function to integrate cues from the local environment to shape vascular organization and blood supply, adapting to ongoing physiological needs in the outer retina.

We observed here that the trophic influence of choroidal macrophages extended also to the maintenance of RPE structure and function. With macrophage depletion, the nature of RPE changes induced has a notable resemblance to structural and functional alterations seen with aging and AMD in the RPE layer, including increased cellular disorganization and decreased cell density in the RPE monolayer (54, 55), increased numbers of multinucleated cells (56), and increased RPE dedifferentiation (57). Previous studies have connected microglia/macrophage activation with RPE alterations, but these had been in pathological situations in which increased production of inflammatory mediators exerts changes on RPE cells (58-60). Contrastingly, our findings here highlight the existence of trophic

macrophage-RPE signaling occurring under normal conditions, suggesting that not only macrophage overaction, but also insufficiency of endogenous macrophage function, may contribute pathogenically to changes in the choroid and RPE layer observed in age-related retinal degeneration.

Our findings highlight the existence of cellular and molecular mechanisms that underlie trophic relationships between choroidal macrophages, choroidal vasculature, and RPE cells. Multiple studies have shown that the maintenance of vasculature in the adult choroid is highly dependent on the nearby presence of viable RPE cells, and specifically on RPE-expressed angiogenic factors (61, 62). Measures that ablate RPE cells (63, 64), or otherwise deplete or prevent the delivery of RPE-derived VEGF (32, 37), resulted in prominent atrophy of choroidal vessels. This dependence of the choroidal vasculature on constitutive RPE support indicates that it is possible that choroidal macrophages may contribute to vascular maintenance indirectly via their effects on RPE cells (Fig. S6). In our experiments, we observed that macrophage depletion resulted in a significant decrease in ratio of VEGF/PEDF factors that are expressed in the RPE-choroidal complex, with a significant decrease in VEGF immunopositivity and an increase of PEDF in the RPE cells layer, indicating that macrophage depletion may induce vascular atrophy by decreasing RPE-mediated angiogenic support. One mode of macrophage-to-RPE signaling that is potentially relevant in this mechanism involves TGFβ; TGFβ ligands, particularly TGFB1, is prominently expressed by tissue macrophages (65, 66). Signaling via TGFBR1/2, which is expressed in RPE cells, has been shown to potentiate RPE production and secretion of VEGF (38, 67). We observed that *Tgfb1* expression is significantly decreased in the RPE-choroidal complex with choroidal depletion, suggesting that TGFB1 secretion by choroidal macrophages to TGBR1/2 on RPE cells may contribute here. Verification of this mode of signaling, as well as other potential modes, await studies involving inducible macrophage-specific loss-of-function interventions in suitable *in vivo* models.

Alternatively, it is possible that macrophage-vasculature signaling may occur directly, and that the RPE structural changes observed here may be secondarily induced by a resulting deficiency of choroidal supply, as suggested by correlative histopathological studies of AMD (49). For example, it has been demonstrated that the choroidal endothelium can signal to the RPE to modulate their tight junctions and barrier functions (68). VEGF-secreting choroidal macrophages can directly potentiate choroidal neovascularization, as demonstrated in experimental studies (49) and suggested by macrophage presence in neovascular membranes in exudative AMD (13). However, our immunohistochemical data do not indicate that macrophages in the healthy choroid constitutively secrete significant levels of VEGF, unlike observations for activated macrophages in choroidal neovascularization (69, 70). Future studies identifying constitutive angiogenic factors expressed by macrophages in the healthy choroid will help address this mechanism of direct macrophage-vascular signaling.

We make the additional discovery that macrophages in the adult choroid, which under normal conditions are non-migratory and demonstrate little constitutive proliferation (11), can be induced by depletion to initiate a regenerative program *de novo*. The cellular source for repopulating macrophages in this context is yet undetermined, and may involve the proliferation of residual resident macrophages, as observed for microglia in the adult retina (21), or the infiltration of circulating monocytes, as occurs in models of retinal injury (71). Our observations here highlight that the regeneration process involves: the *in situ* proliferation of repopulating cells in the choroid, morphological and marker maturation during repopulation, and an accurate recapitulation of original macrophage density, distribution, and

morphology, akin to the repopulation of microglia in the retina (21) and brain (52). The ability of regenerated macrophages to recapitulate the endogenous function of the original macrophages is evidenced here by the arrest of choroidal vascular atrophy and RPE degenerative change, and recovery of angiogenic factor balance upon the full restoration of macrophage numbers in the choroid. Interestingly, we did not observe a complete reversal of vascular and RPE degenerative changes that recovers the original, pre-depletion anatomy in the RPE-choroid, suggesting that aspects of degenerative change may be permanent and resist restoration by reinstituted trophic signals. This ability to regenerate choroidal macrophages presents a new potential therapeutic opportunity for immune modulation in the choroid in which depletion-repopulation measures may be employed to "reset" the immune environment in the choroid in pathological situations in which choroidal macrophages demonstrate chronic activation. The feasibility of this approach will require further elucidation of the nature of macrophage repopulation in models of retinal pathology.

Taken together, our results here have significant relevance to understanding choroidal degeneration in aging and AMD progression (2) and to ongoing translational efforts to preserve or restore the vascular choroid in age-related disease (18). Additional to the concept that abnormal and imbalanced immune activation within the choroid involving proinflammatory and complement-mediated mechanisms can exert deleterious effects on choroidal vascular structure, our findings show that non-inflammatory trophic influences from resident choroidal macrophages may be additionally important in maintaining choroidal structural integrity across the lifespan of the organism. Our findings suggest that age- and AMD-associated degeneration in the RPE-choroid complex may be contributed to by multiple immune influences that combine inappropriate inflammatory activation and insufficient trophic support. The balance between these possibly simultaneous mechanisms may influence the relative severity of degeneration between the choriocapillaris vs. the adjacent RPE layer, which may influence the progression to the atrophic vs. the neovascular forms of AMD as hypothesized from histopathological studies (49). As such, immunomodulatory interventions aimed at preserving the integrity of the RPE-choroid complex should optimally enable both increased macrophage trophic influences and decreased inflammatory damage. These perspectives add to the strategy of choroidal macrophage-targeted interventions as potential therapies aimed at choroidal preservation in diseases like age-related macular degeneration.

References

1. Fields MA, Del Priore LV, Adelman RA, & Rizzolo LJ (2019) Interactions of the choroid, Bruch's membrane, retinal pigment epithelium, and neurosensory retina collaborate to form the outer blood-retinal-barrier. *Prog Retin Eye Res*:100803.
2. Arya M, Sabrosa AS, Duker JS, & Waheed NK (2018) Choriocapillaris changes in dry age-related macular degeneration and geographic atrophy: a review. *Eye Vis (Lond)* 5:22.
3. Sohn EH*, et al.* (2019) Choriocapillaris Degeneration in Geographic Atrophy. *Am J Pathol* 189(7):1473-1480.
4. Bourne RRA*, et al.* (2018) Prevalence and causes of vision loss in high-income countries and in Eastern and Central Europe in 2015: magnitude, temporal trends and projections. *Br J Ophthalmol* 102(5):575-585.
5. Keenan TD*, et al.* (2019) Choroidal Thickness and Vascularity Vary with Disease Severity and Subretinal Drusenoid Deposit Presence in Nonadvanced Age-Related Macular Degeneration. *Retina*.
6. Spaide RF (2009) Age-related choroidal atrophy. *Am J Ophthalmol* 147(5):801-810.
7. Van Hove H*, et al.* (2019) A single-cell atlas of mouse brain macrophages reveals unique transcriptional identities shaped by ontogeny and tissue environment. *Nat Neurosci* 22(6):1021-1035.
8. McMenamin PG (1999) Distribution and phenotype of dendritic cells and resident tissue macrophages in the dura mater, leptomeninges, and choroid plexus of the rat brain as demonstrated in wholemount preparations. *J Comp Neurol* 405(4):553-562.
9. McMenamin PG (1999) Dendritic cells and macrophages in the uveal tract of the normal mouse eye. *Br J Ophthalmol* 83(5):598-604.
10. Forrester JV, Xu H, Kuffova L, Dick AD, & McMenamin PG (2010) Dendritic cell physiology and function in the eye. *Immunol Rev* 234(1):282-304.
11. Kumar A, Zhao L, Fariss RN, McMenamin PG, & Wong WT (2014) Vascular associations and dynamic process motility in perivascular myeloid cells of the mouse choroid: implications for function and senescent change. *Invest Ophthalmol Vis Sci* 55(3):1787-1796.
12. Jiang HR, Lumsden L, & Forrester JV (1999) Macrophages and dendritic cells in IRBP-induced experimental autoimmune uveoretinitis in B10RIII mice. *Invest Ophthalmol Vis Sci* 40(13):3177-3185.
13. Cherepanoff S, McMenamin P, Gillies MC, Kettle E, & Sarks SH (2010) Bruch's membrane and choroidal macrophages in early and advanced age-related macular degeneration. *Br J Ophthalmol* 94(7):918-925.
14. McLeod DS*, et al.* (2016) Distribution and Quantification of Choroidal Macrophages in Human Eyes With Age-Related Macular Degeneration. *Invest Ophthalmol Vis Sci* 57(14):5843-5855.
15. Lengyel I*, et al.* (2004) Association of drusen deposition with choroidal intercapillary pillars in the aging human eye. *Invest Ophthalmol Vis Sci* 45(9):2886-2892.
16. Mullins RF, Johnson MN, Faidley EA, Skeie JM, & Huang J (2011) Choriocapillaris vascular dropout related to density of drusen in human eyes with early age-related macular degeneration. *Invest Ophthalmol Vis Sci* 52(3):1606-1612.
17. Biesemeier A, Taubitz T, Julien S, Yoeruek E, & Schraermeyer U (2014) Choriocapillaris breakdown precedes retinal degeneration in age-related macular degeneration. *Neurobiol Aging* 35(11):2562-2573.
18. Whitmore SS*, et al.* (2015) Complement activation and choriocapillaris loss in early AMD: implications for pathophysiology and therapy. *Prog Retin Eye Res* 45:1-29.

19. Coleman DJ*, et al.* (2018) Treatment of Macular Degeneration with Sildenafil: Results of a Two-Year Trial. *Ophthalmologica* 240(1):45-54.
20. Condren AB*, et al.* (2013) Perivascular mural cells of the mouse choroid demonstrate morphological diversity that is correlated to vasoregulatory function. *PLoS One* 8(1):e53386.
21. Zhang Y*, et al.* (2018) Repopulating retinal microglia restore endogenous organization and function under CX3CL1-CX3CR1 regulation. *Sci Adv* 4(3):eaap8492.
22. Sharma R*, et al.* (2019) Clinical-grade stem cell-derived retinal pigment epithelium patch rescues retinal degeneration in rodents and pigs. *Sci Transl Med* 11(475).
23. Ogilvy AJ, Shen D, Wang Y, Chan CC, & Abu-Asab MS (2014) Implications of DNA leakage in eyes of mutant mice. *Ultrastruct Pathol* 38(5):335-343.
24. MacDonald KP*, et al.* (2010) An antibody against the colony-stimulating factor 1 receptor depletes the resident subset of monocytes and tissue- and tumor-associated macrophages but does not inhibit inflammation. *Blood* 116(19):3955-3963.
25. Sakurai E, Anand A, Ambati BK, van Rooijen N, & Ambati J (2003) Macrophage depletion inhibits experimental choroidal neovascularization. *Invest Ophthalmol Vis Sci* 44(8):3578-3585.
26. Jarosz-Biej M*, et al.* (2018) M1-like macrophages change tumor blood vessels and microenvironment in murine melanoma. *PLoS One* 13(1):e0191012.
27. Wang X*, et al.* (2016) Requirement for Microglia for the Maintenance of Synaptic Function and Integrity in the Mature Retina. *J Neurosci* 36(9):2827-2842.
28. Shi YY*, et al.* (2011) Monocyte/macrophages promote vasculogenesis in choroidal neovascularization in mice by stimulating SDF-1 expression in RPE cells. *Graefes Arch Clin Exp Ophthalmol* 249(11):1667-1679.
29. Wang JC*, et al.* (2015) CFH Y402H polymorphism is associated with elevated vitreal GM-CSF and choroidal macrophages in the postmortem human eye. *Mol Vis* 21:264-272.
30. Redmond TM*, et al.* (1998) Rpe65 is necessary for production of 11-cis-vitamin A in the retinal visual cycle. *Nat Genet* 20(4):344-351.
31. Kurihara T, Westenskow PD, Bravo S, Aguilar E, & Friedlander M (2012) Targeted deletion of Vegfa in adult mice induces vision loss. *J Clin Invest* 122(11):4213-4217.
32. Saint-Geniez M, Kurihara T, Sekiyama E, Maldonado AE, & D'Amore PA (2009) An essential role for RPE-derived soluble VEGF in the maintenance of the choriocapillaris. *Proc Natl Acad Sci U S A* 106(44):18751-18756.
33. Mori K*, et al.* (2001) Pigment epithelium-derived factor inhibits retinal and choroidal neovascularization. *J Cell Physiol* 188(2):253-263.
34. Amaral J & Becerra SP (2010) Effects of human recombinant PEDF protein and PEDF-derived peptide 34-mer on choroidal neovascularization. *Invest Ophthalmol Vis Sci* 51(3):1318-1326.
35. Lindahl P, Johansson BR, Leveen P, & Betsholtz C (1997) Pericyte loss and microaneurysm formation in PDGF-B-deficient mice. *Science* 277(5323):242-245.
36. Pollina EA*, et al.* (2008) Regulating the angiogenic balance in tissues. *Cell Cycle* 7(13):2056-2070.
37. Marneros AG*, et al.* (2005) Vascular endothelial growth factor expression in the retinal pigment epithelium is essential for choriocapillaris development and visual function. *Am J Pathol* 167(5):1451-1459.
38. Nagineni CN*, et al.* (2003) Transforming growth factor-beta induces expression of vascular endothelial growth factor in human retinal pigment epithelial cells: involvement of mitogen-activated protein kinases. *J Cell Physiol* 197(3):453-462.
39. Huang Y*, et al.* (2018) Repopulated microglia are solely derived from the proliferation of residual microglia after acute depletion. *Nat Neurosci* 21(4):530-540.
40. Wynn TA, Chawla A, & Pollard JW (2013) Macrophage biology in development, homeostasis and disease. *Nature* 496(7446):445-455.

41. Wolf SA, Boddeke HW, & Kettenmann H (2017) Microglia in Physiology and Disease. *Annu Rev Physiol* 79:619-643.
42. Li Q & Barres BA (2018) Microglia and macrophages in brain homeostasis and disease. *Nat Rev Immunol* 18(4):225-242.
43. McMenamin PG, Saban DR, & Dando SJ (2019) Immune cells in the retina and choroid: Two different tissue environments that require different defenses and surveillance. *Prog Retin Eye Res* 70:85-98.
44. Wakatsuki Y, Shinojima A, Kawamura A, & Yuzawa M (2015) Correlation of Aging and Segmental Choroidal Thickness Measurement using Swept Source Optical Coherence Tomography in Healthy Eyes. *PLoS One* 10(12):e0144156.
45. Zhang C*, et al.* (2014) Assessment of choroidal thickness in healthy and glaucomatous eyes using swept source optical coherence tomography. *PLoS One* 9(10):e109683.
46. Abbey AM*, et al.* (2015) Optical coherence tomography measurements of choroidal thickness in healthy eyes: correlation with age and axial length. *Ophthalmic Surg Lasers Imaging Retina* 46(1):18-24.
47. Bhutto I & Lutty G (2012) Understanding age-related macular degeneration (AMD): relationships between the photoreceptor/retinal pigment epithelium/Bruch's membrane/choriocapillaris complex. *Mol Aspects Med* 33(4):295-317.
48. Chirco KR, Sohn EH, Stone EM, Tucker BA, & Mullins RF (2017) Structural and molecular changes in the aging choroid: implications for age-related macular degeneration. *Eye (Lond)* 31(1):10-25.
49. Seddon JM*, et al.* (2016) Histopathological Insights Into Choroidal Vascular Loss in Clinically Documented Cases of Age-Related Macular Degeneration. *JAMA Ophthalmol* 134(11):1272-1280.
50. Stefater JA, 3rd*, et al.* (2011) Regulation of angiogenesis by a non-canonical Wnt-Flt1 pathway in myeloid cells. *Nature* 474(7352):511-515.
51. Arnold T & Betsholtz C (2013) The importance of microglia in the development of the vasculature in the central nervous system. *Vasc Cell* 5(1):4.
52. Elmore MR*, et al.* (2014) Colony-stimulating factor 1 receptor signaling is necessary for microglia viability, unmasking a microglia progenitor cell in the adult brain. *Neuron* 82(2):380-397.
53. De Schepper S*, et al.* (2018) Self-Maintaining Gut Macrophages Are Essential for Intestinal Homeostasis. *Cell* 175(2):400-415 e413.
54. Del Priore LV, Kuo YH, & Tezel TH (2002) Age-related changes in human RPE cell density and apoptosis proportion in situ. *Invest Ophthalmol Vis Sci* 43(10):3312-3318.
55. Bhatia SK*, et al.* (2016) Analysis of RPE morphometry in human eyes. *Mol Vis* 22:898-916.
56. Chen M*, et al.* (2016) Retinal pigment epithelial cell multinucleation in the aging eye - a mechanism to repair damage and maintain homoeostasis. *Aging Cell* 15(3):436-445.
57. Makarev E*, et al.* (2014) Pathway activation profiling reveals new insights into age-related macular degeneration and provides avenues for therapeutic interventions. *Aging (Albany NY)* 6(12):1064-1075.
58. Kutty RK*, et al.* (2016) Proinflammatory cytokines decrease the expression of genes critical for RPE function. *Mol Vis* 22:1156-1168.
59. Yamawaki T*, et al.* (2016) The Ingenious Interactions Between Macrophages and Functionally Plastic Retinal Pigment Epithelium Cells. *Invest Ophthalmol Vis Sci* 57(14):5945-5953.
60. Ma W, Zhao L, Fontainhas AM, Fariss RN, & Wong WT (2009) Microglia in the mouse retina alter the structure and function of retinal pigmented epithelial cells: a potential cellular interaction relevant to AMD. *PLoS One* 4(11):e7945.

61. Blaauwgeers HG*, et al.* (1999) Polarized vascular endothelial growth factor secretion by human retinal pigment epithelium and localization of vascular endothelial growth factor receptors on the inner choriocapillaris. Evidence for a trophic paracrine relation. *Am J Pathol* 155(2):421-428.
62. Saint-Geniez M, Maldonado AE, & D'Amore PA (2006) VEGF expression and receptor activation in the choroid during development and in the adult. *Invest Ophthalmol Vis Sci* 47(7):3135-3142.
63. Hayashi A*, et al.* (1999) Surgically induced degeneration and regeneration of the choriocapillaris in rabbit. *Graefes Arch Clin Exp Ophthalmol* 237(8):668-677.
64. Korte GE, Reppucci V, & Henkind P (1984) RPE destruction causes choriocapillary atrophy. *Invest Ophthalmol Vis Sci* 25(10):1135-1145.
65. Kwong KY*, et al.* (2006) Expression of transforming growth factor beta (TGF-b1) by human preterm lung inflammatory cells. *Life Sci* 79(25):2349-2356.
66. Huen SC, Moeckel GW, & Cantley LG (2013) Macrophage-specific deletion of transforming growth factor-beta1 does not prevent renal fibrosis after severe ischemia-reperfusion or obstructive injury. *Am J Physiol Renal Physiol* 305(4):F477-484.
67. Bian ZM, Elner SG, & Elner VM (2007) Regulation of VEGF mRNA expression and protein secretion by TGF-beta2 in human retinal pigment epithelial cells. *Exp Eye Res* 84(5):812-822.
68. Benedicto I*, et al.* (2017) Concerted regulation of retinal pigment epithelium basement membrane and barrier function by angiocrine factors. *Nat Commun* 8:15374.
69. Grossniklaus HE*, et al.* (2002) Macrophage and retinal pigment epithelium expression of angiogenic cytokines in choroidal neovascularization. *Mol Vis* 8:119-126.
70. Ishibashi T*, et al.* (1997) Expression of vascular endothelial growth factor in experimental choroidal neovascularization. *Graefes Arch Clin Exp Ophthalmol* 235(3):159-167.
71. Ma W*, et al.* (2017) Monocyte infiltration and proliferation reestablish myeloid cell homeostasis in the mouse retina following retinal pigment epithelial cell injury. *Sci Rep* 7(1):8433.

Figure Legends

Figure 1. CSF1R inhibition via PLX5622 administration induces a rapid and sustained depletion of resident macrophages in the adult mouse choroid. (A) Three-month old wild type Balb/cJ mice were administered diet containing PLX5622 (at 1200 parts per million) continuously for up to 7 weeks. Controls consisted of age-matched animals maintained on standard mouse chow. Resident macrophages in the choroid were visualized by immunohistochemical staining for MHCII (*green*) and IBA1 (*red*) in sclerochoroidal flatmounts. Panels show representative images with insets showing high-magnification views. Ellipses mark the position of the optic nerve. The choroid of control animals demonstrated a dense network of IBA1+, MHCII+ resident macrophages with ramified, dendritiform morphology. Macrophage numbers were markedly decreased following 1 week of PLX5622 administration which remained reduced at similar levels for up to 7 weeks of administration. The few residual macrophages showed reduced ramification. Scale bar = 500 µm. **(B)** Quantitative counts of total MHC-II^{+} macrophages across the entire choroid revealed a ≈90% reduction in macrophage numbers by 1 week of PLX5622 treatment, which was sustained with continued treatment. **(C)** Quantitative PCR analyses of the whole RPE-choroid complex demonstrated a corresponding reduction in the expression of *Iba1* mRNA, corresponding to the depletion of Iba1-expressing macrophages. P values indicate comparisons relative to control, 1-way ANOVA, n = 4 animals per treatment group.

Figure 2. Long-term depletion of resident choroidal macrophages results in progressive choroidal thinning and vascular atrophy. (A) Animals administered PLX5622-containing diet continuously over 7 weeks were followed with longitudinal *in vivo* enhanced depth imaging optical coherence tomography (EDI OCT) imaging; I-bars show the measurements made of choroidal thickness. Scale bar = 100 µm. **(B)** Choroidal thicknesses measured in the temporal and nasal quadrants (at 300 µm temporal and nasal respectively from the optic nerve at the horizontal meridian) demonstrated progressive and significant decreases from baseline. **(C)** Total retinal thickness (measured from the RPE layer to the vitreal surface at the internal limiting membrane) were stable over the same period. P values in B, C were computed for comparisons relative to baseline using 1-way ANOVA test, n = 10 eyes from 5 animals at each time-points. **(D-F)** Comparative histological analysis of the choroid in control and depleted animals showed decreases in overall choroidal thickness and vascular density. Panels show representative images with insets (*yellow boxes*) showing high-magnification views. Scale bar = 50 µm. Mean total choroidal thickness was significantly reduced with macrophage depletion **(E)**, as was the mean cross-sectional area of vascular lumina **(F)**, with a trend towards decreased density of choroidal vessels. n=6 eyes from 3 animals per treatment group. **(G, H)** Choriocapillaris vascular structure was imaged in flat-mounted sclerochoroidal tissue following vascular labeling with DiI perfusion; the fractional area coverage by vessels in the choriocapillaris was significantly reduced following 7 weeks of macrophage depletion. Scale bar = 50 µm. n=8 eyes from 4 animals per treatment group. P values in **E**, **F**, and **H** were computed with an unpaired t-test with Welch's correction.

Figure 3. Long-term depletion of choroidal macrophages induces alterations in RPE structure and function. (A) Immunohistochemical analyses of the RPE monolayer in sclerochoroidal flatmounts in control and PLX5622-treated animals (for 7 weeks) were performed with RPE65 *(green)*, conjugated phalloidin to stain F-actin *(red)*, and DAPI *(blue)*. High-magnification views (yellow box inset) highlight large multinucleated (>3 nuclei) cells (*asterisk **), local reductions of RPE65 immunopositivity (*arrow*), and generally increased intracellular vacuolation. Scale bar = 20 µm. **(B)** Quantitative analysis of RPE65 immunopositivity in RPE. **(C)** Transmission electron microscopic analysis of RPE cells show in PLX5622-

treated animals disrupted RPE apical microvilli structure (*arrow*) and increased intracellular vacuolation (*arrowhead*). Quantitative comparison of RPE morphological features from control and depleted animals of **(D)** RPE cell density, mean and distribution, and **(E)** the proportion of multinucleated (≥3 nuclei), mononucleated and binucleated RPE cells. P values in B, D, E correspond to comparisons made using an unpaired t-test with Welch's correction. n = 4 to 6 animals in each treatment group. **(F)** Comparison of scotopic electroretinographic responses between control and depleted animals showed significantly decreased a- and b-wave amplitudes in the PLX5622-treated group. P values correspond to comparisons made using a 2-way ANOVA test, n = 10 to 16 eyes from 5 to 8 animals in each treatment group.

Figure 4. Expression levels of angiogenic growth factors in the RPE-choroid complex are altered with long-term choroidal macrophage depletion. Total mRNA and protein were isolated from RPE-choroid complexes of animals treated with PLX5622-containing diet for 1 or 7 weeks and untreated control animals. mRNA levels of *Vegfa* and *Vegfc* **(A)**, and protein level of VEGF **(B)** were all significantly reduced following 7 weeks of depletion. Immunohistochemical localization demonstrated VEGF expression at the level of the RPE that was decreased following macrophage depletion **(C)**. *Pedf* mRNA **(D)** and PEDF protein **(E)** were increased following macrophage depletion; immunohistochemical analyses demonstrated increased PEDF immunopositivity in the RPE layer and choroid **(F)**. *Pdgfa* and *Pdgfb* mRNA levels **(G)** and PDGF-AA and PDGF-BB protein levels **(H)** were largely unaltered with macrophage depletion. P values were from a 1-way ANOVA, n = 4 to 8 animals per treatment group.

Figure 5. Choroidal macrophages demonstrate spontaneous repopulation and recovery of constitutive numbers following depletion. (A) Adult 3-month old mice were administered a diet containing PLX5622 for 3 weeks to achieve depletion of choroidal macrophages (depletion phase), and then returned to a standard diet for another 4 weeks (repopulation phase). The control group consisted of age-matched animals maintained on a standard diet. **(B)** Sclerochoroidal flatmounts were immunolabeled with MHCII *(green)* and IBA1 *(red)* to visualize the resident macrophages. Panels show representative images and yellow box marking the areas showing high-magnification views. Scale bar = 1mm. **(C)** The total number of macrophages in the choroid that were immunopositive for both IBA1 and MHCII markedly decreased after 3 weeks of PLX5622 administration but progressively increased following PLX5622 cessation to reach baseline levels after 4-6 weeks. **(D)** While all IBA1+ macrophages were immunopositive for MHC at baseline, a small fraction of IBA1+ macrophages were immunonegative for MHCII early in the repopulation phase (at 1 week following resumption of a standard diet). This phenotype was transient as all IBA1+ macrophages reacquired MHCII immunopositivity when repopulation neared completion at 6 weeks of repopulation. P values were from a 1-way ANOVA, n = 3 animals per treatment group.

Figure 6. Choroidal macrophage repopulation following depletion arrests depletion-associated choroidal vascular atrophy. (A) Experimental plan for the assessment of vascular changes in the choroid during macrophage depletion and repopulation. Age-matched 3 month-old adult BALB/cJ animals were divided into two groups: (1) the depletion-repopulation group: animals administered PLX5622-containing diet for 3 weeks, followed by 4 weeks on a standard diet, and (2) the continuous depletion group: animals were administered PLX5622-containing diet continuously for 7 weeks. Animals in both groups were assessed at baseline, and 1, 3, 5, and 7 weeks following baseline with serial OCT imaging. **(B)** Representative longitudinal aligned *in vivo* EDI OCT images of animals in the two groups taken at different time points; bars show the intervals across which choroidal thickness were measured. Scale bar = 200 µm. Choroidal thicknesses measured in the temporal and nasal quadrants (at 300 µm temporal

and nasal respectively from the optic nerve at the horizontal meridian) decreased progressively with time in the continuously depleted group (*red* line), but stabilized in the depletion/repopulation group (*green* line) upon the onset of repopulation at 3 weeks following baseline, n = 9 eyes from 5 animals in each group for all time-points, p values indicate comparisons between the two experimental groups, 2-way ANOVA using a mixed-effects analysis. **(C)** Choriocapillaris vascular structure was imaged in sclerochoroidal flatmounts labeled with systemic DiI perfusion. Scale bar = 50 µm. The fractional area coverage by choriocapillaris vessels decreased continuously up to 7 weeks following baseline in the continuous depletion group but was stabilized from 3 to 7 weeks following baseline in the depletion/repopulation group. P values were from a 1-way ANOVA, n=8 eyes from 4 animals per treatment group.

Figure 7. Choroidal macrophage repopulation following depletion arrests depletion-associated alterations in RPE structure and gene expression. (A) Immunohistochemical analyses of the RPE-sclerochoroidal flatmounts from (1) untreated control animals (*white* bars), (2) animals continuously treated for 3 weeks of PLX5622-containing diet (*pink* bars), (3) animals continuously treated for 7 weeks of PLX5622-containing diet (*red* bars), and (4) animals treated for 3 weeks of PLX5622 containing diet and then followed by 4 weeks of standard diet (*green* bars); were performed with RPE65 *(green)*, conjugated phalloidin *(red)*, and DAPI *(blue)*. The progressive patchy decrease in RPE65 immunopositivity and increase of large multinucleated (≥3 nuclei) cells were observed in animals in the 3- and 7-weeks depletion groups, however these changes were recovered upon the onset of repopulation. High-magnification views in the inset (yellow boxes) demonstrated the presence of large cells (>500 µm^2 in area, asterisks) with multiple nuclei in the 7-week depleted group but was less prominent in the repopulated group. **(B)** Quantitative analysis of RPE morphology revealed that repopulation of choroidal macrophages after 3 weeks of depletion prevented further decrease in RPE cell density evident on 7 weeks of depletion. **(C)** Analysis of the distribution of RPE cell areas revealed that the increase in the proportion of large cells (>500 µm^2 in area) induced with 7 weeks depletion was prevented in the repopulation group, which resembled the control and 3-week depletion groups in their distribution. **(D)** Analysis of the proportion of multinucleated RPE cells (≥ 3 nuclei) showed that the increased proportion of multinucleated cells induced with 7 weeks depletion was prevented in the repopulation group. **(E)** Quantitation of mean intensity of RPE65 immunopositivity showed that the significant decrease in RPE65 staining induced by depletion was partially restored after macrophage repopulation. P values indicate comparisons computed from a 1-way ANOVA, n = analysis of 4 imaging field from each animal, 4 animals per treatment group.

Figure 8. Alterations in angiogenic factor expression induced by macrophage depletion are reversed upon macrophage repopulation. mRNA and total protein were isolated from the RPE-choroid complex of (1) control animals maintained on a standard diet (*white* bars), (2) depleted animals treated continuously with a PLX5622-containing diet for 7 weeks (*red* bars), and (3) repopulated animals treated with PLX5622-containing diet for 3 weeks and then switched to a standard diet for 4 weeks (*green* bars). mRNA and protein levels of angiogenic factors were analyzed by qrt-PCR and multiplex assay/ELISA respectively. **(A)** mRNA levels of *Vegfa* and *Vegfc*, and protein level of VEGFA, which were all decreased in the depleted group relative to the control group, were recovered back to control levels in the repopulated group. **(B)** mRNA levels of *Pedf*, and protein levels of PEDF, which were increased in the depleted group relative to the control group, were found at intermediate levels in the repopulated group. P values were from a 1-way ANOVA, n = 4 to 6 animals per treatment group.

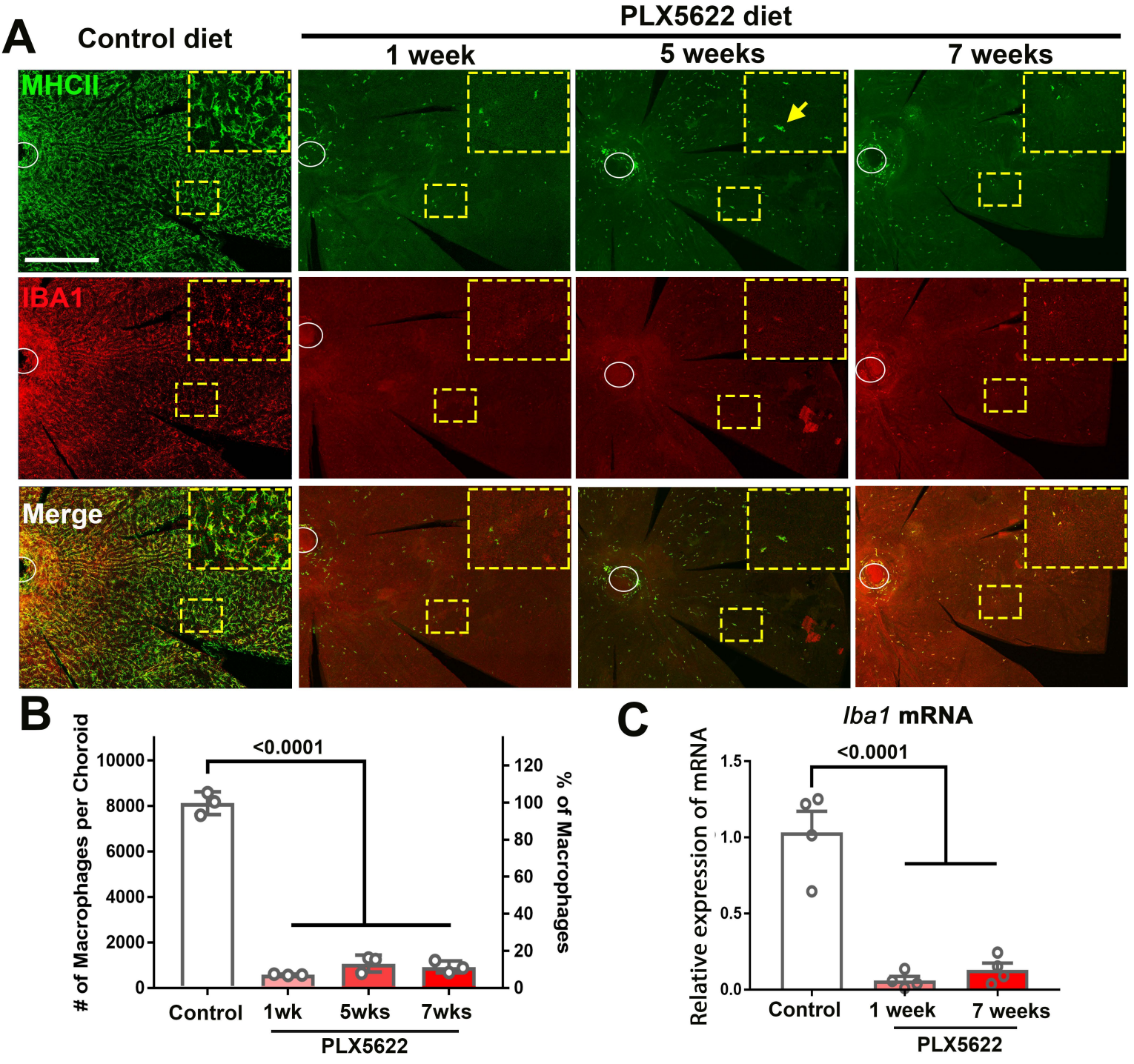
A
Control diet
PLX5622 diet
1 week
5 weeks
7 weeks
MHCII
IBA1
Merge
B
# of Macrophages per Choroid
% of Macrophages
<0.0001
Control
1wk
5wks
7wks
PLX5622
C
Iba1 mRNA
Relative expression of mRNA
<0.0001
Control
1 week
7 weeks
PLX5622

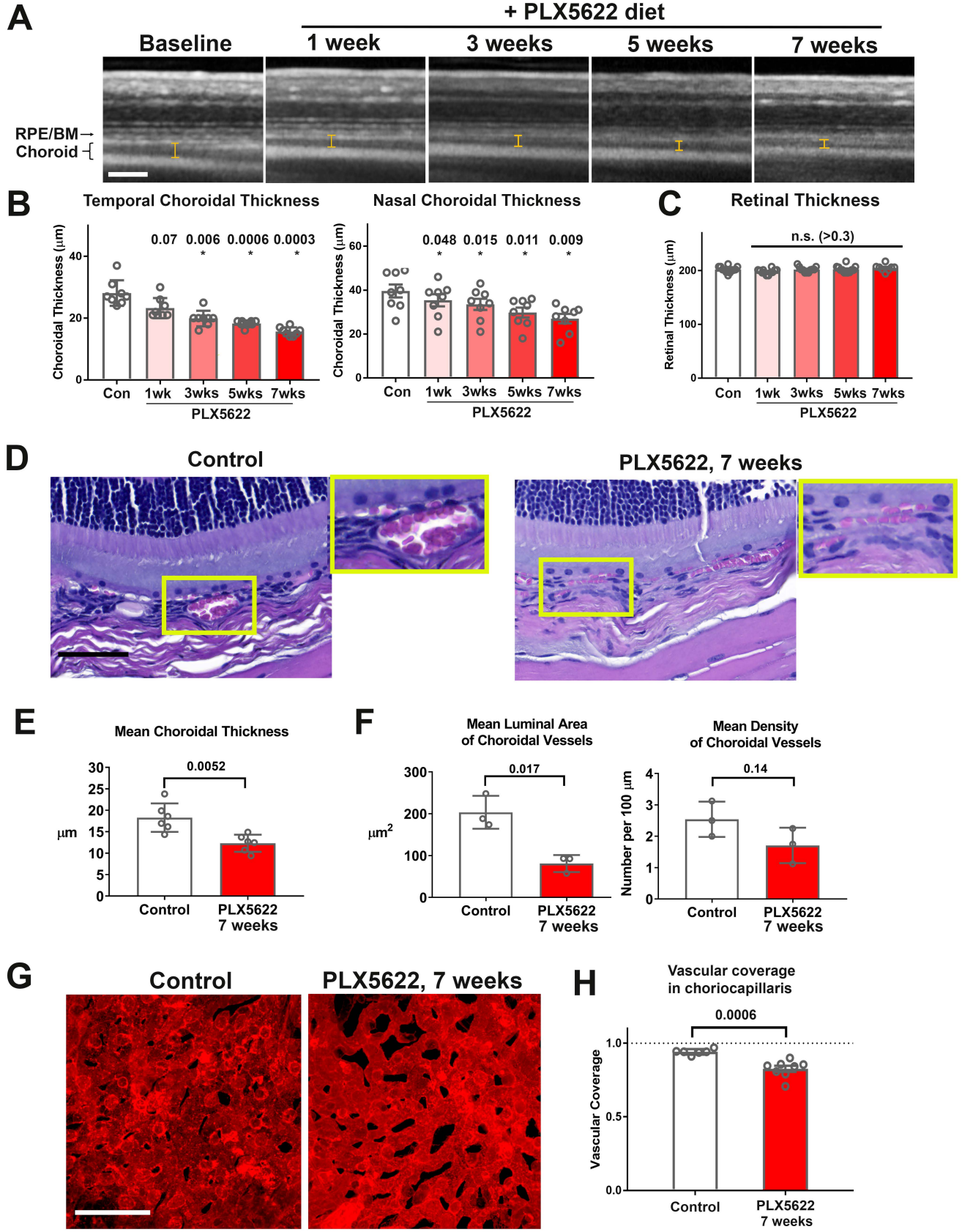
A
+ PLX5622 diet
Baseline
1 week
3 weeks
5 weeks
7 weeks
RPE/BM
Choroid
B
Temporal Choroidal Thickness
Choroidal Thickness (µm)
0.07
0.006
0.0006
0.0003
Con
1wk
3wks
5wks
7wks
PLX5622
Nasal Choroidal Thickness
0.048
0.015
0.011
0.009
C
Retinal Thickness
Retinal Thickness (µm)
n.s. (>0.3)
D
Control
PLX5622, 7 weeks
E
Mean Choroidal Thickness
0.0052
µm
Control
PLX5622
7 weeks
F
Mean Luminal Area
of Choroidal Vessels
0.017
µm2
Mean Density
of Choroidal Vessels
0.14
Number per 100 µm
G
Control
PLX5622, 7 weeks
H
Vascular coverage
in choriocapillaris
0.0006
Vascular Coverage

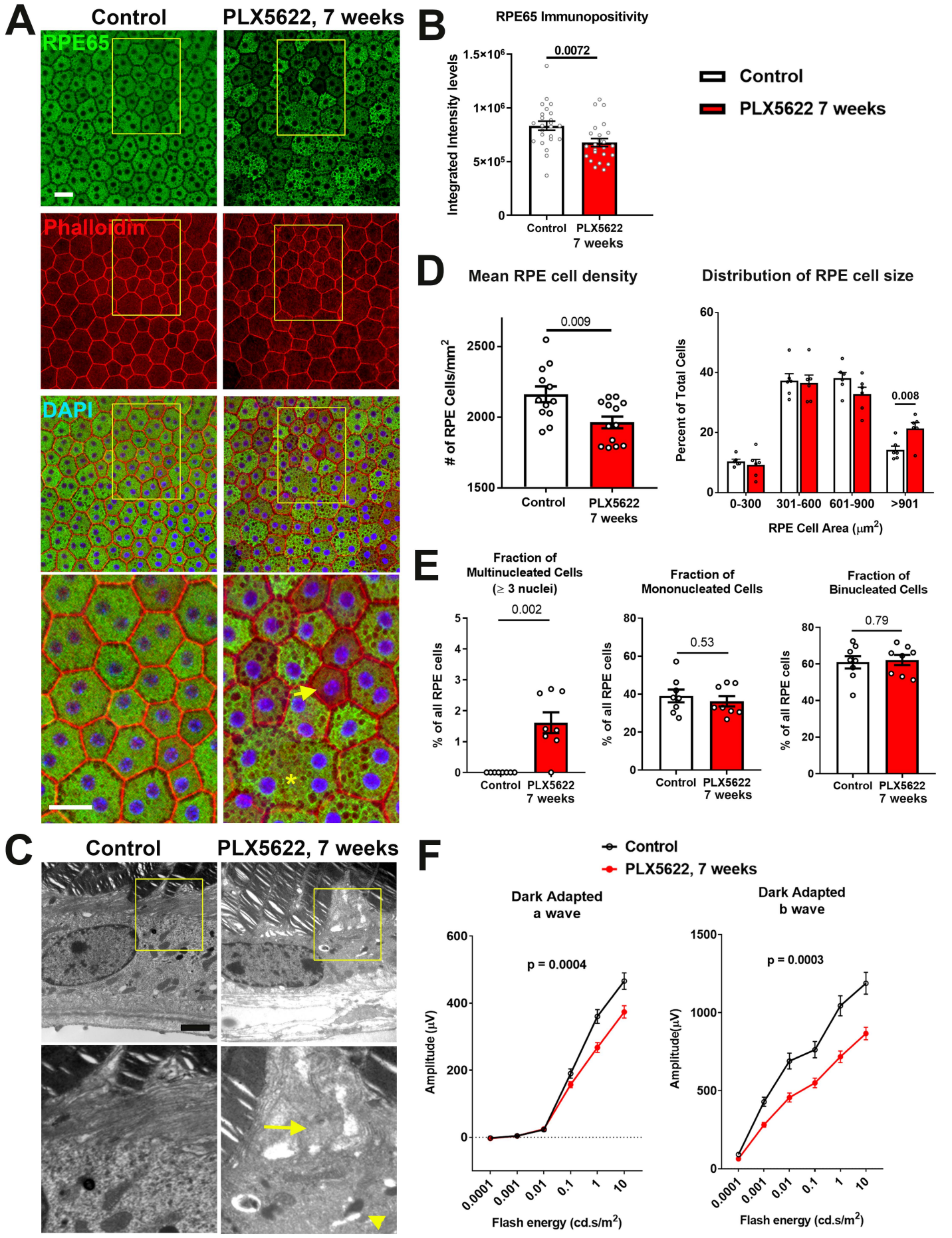
A
Control
PLX5622, 7 weeks
RPE65
Phalloidin
DAPI
B
RPE65 Immunopositivity
0.0072
Integrated Intensity levels
1.5×10⁶
1×10⁶
5×10⁵
0
Control
PLX5622
7 weeks
Control
PLX5622 7 weeks
D
Mean RPE cell density
0.009
# of RPE Cells/mm²
2500
2000
1500
Control
PLX5622
7 weeks
Distribution of RPE cell size
Percent of Total Cells
60
40
20
0
0.008
0-300
301-600
601-900
>901
RPE Cell Area (μm²)
E
Fraction of Multinucleated Cells (≥ 3 nuclei)
0.002
% of all RPE cells
5
4
3
2
1
0
Control
PLX5622
7 weeks
Fraction of Mononucleated Cells
0.53
80
60
40
20
0
Fraction of Binucleated Cells
0.79
C
Control
PLX5622, 7 weeks
F
Control
PLX5622, 7 weeks
Dark Adapted a wave
p = 0.0004
Amplitude (μV)
600
400
200
0
0.0001
0.001
0.01
0.1
1
10
Flash energy (cd.s/m²)
Dark Adapted b wave
p = 0.0003
Amplitude(μV)
1500
1000
500
0
Flash energy (cd.s/m²)

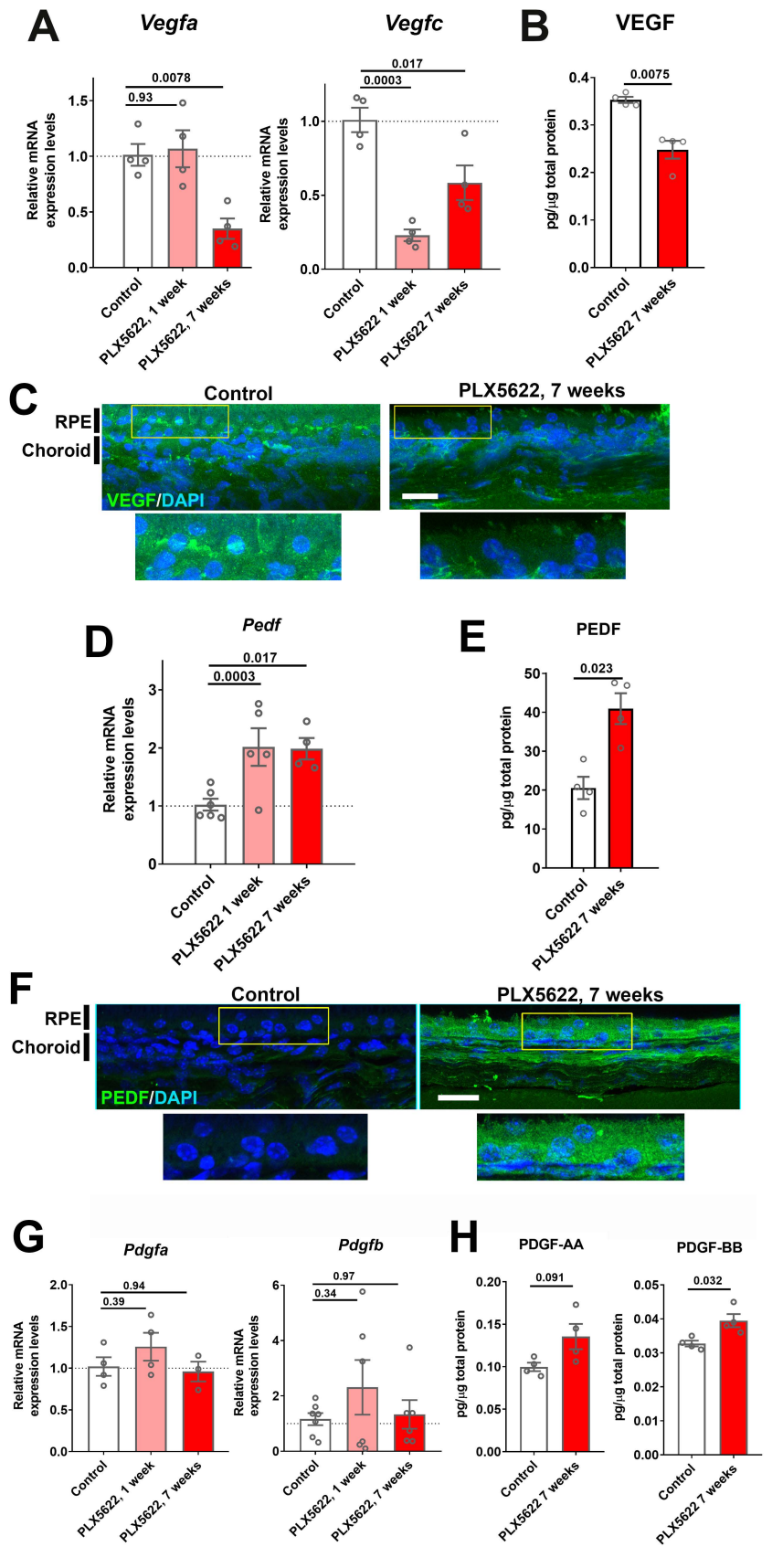
A
Vegfa
Relative mRNA expression levels
0.0078
0.93
Control
PLX5622, 1 week
PLX5622, 7 weeks
Vegfc
0.017
0.0003
PLX5622 1 week
PLX5622 7 weeks
B
VEGF
pg/μg total protein
0.0075
C
Control
PLX5622, 7 weeks
RPE
Choroid
VEGF/DAPI
D
Pedf
E
PEDF
0.023
PEDF/DAPI
F
G
Pdgfa
0.94
0.39
Pdgfb
0.97
0.34
H
PDGF-AA
0.091
PDGF-BB
0.032

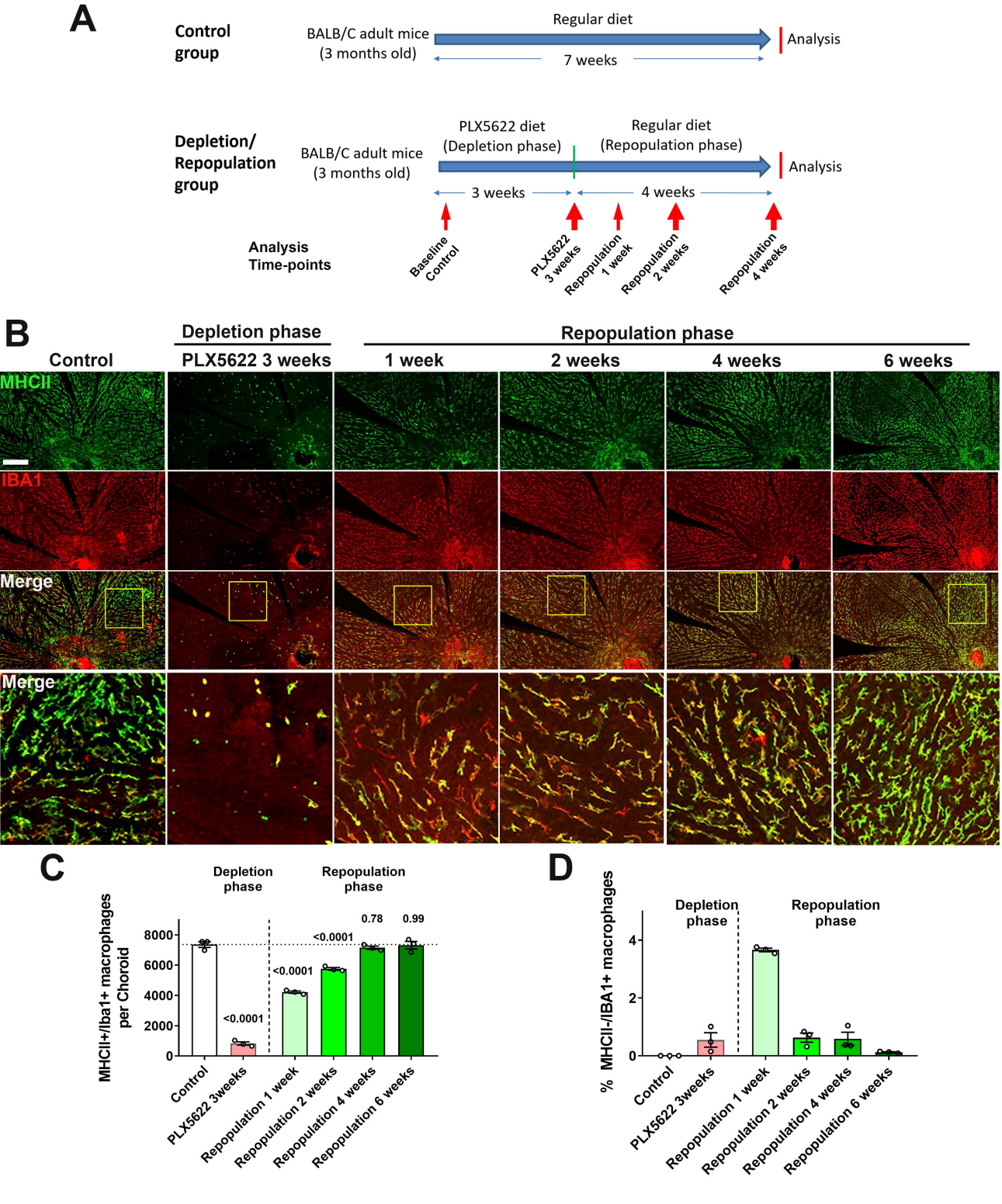
A
Control group
BALB/C adult mice (3 months old)
Regular diet
7 weeks
Analysis
Depletion/ Repopulation group
BALB/C adult mice (3 months old)
PLX5622 diet (Depletion phase)
Regular diet (Repopulation phase)
3 weeks
4 weeks
Analysis
Analysis Time-points
Baseline Control
PLX5622 3 weeks
Repopulation 1 week
Repopulation 2 weeks
Repopulation 4 weeks
B
Depletion phase
Repopulation phase
Control
PLX5622 3 weeks
1 week
2 weeks
4 weeks
6 weeks
MHCII
IBA1
Merge
Merge
C
Depletion phase
Repopulation phase
MHCII+/Iba1+ macrophages per Choroid
8000
6000
4000
2000
0
<0.0001
<0.0001
<0.0001
0.78
0.99
Control
PLX5622 3weeks
Repopulation 1 week
Repopulation 2 weeks
Repopulation 4 weeks
Repopulation 6 weeks
D
Depletion phase
Repopulation phase
% MHCII-/IBA1+ macrophages
4
2
0
Control
PLX5622 3weeks
Repopulation 1 week
Repopulation 2 weeks
Repopulation 4 weeks
Repopulation 6 weeks

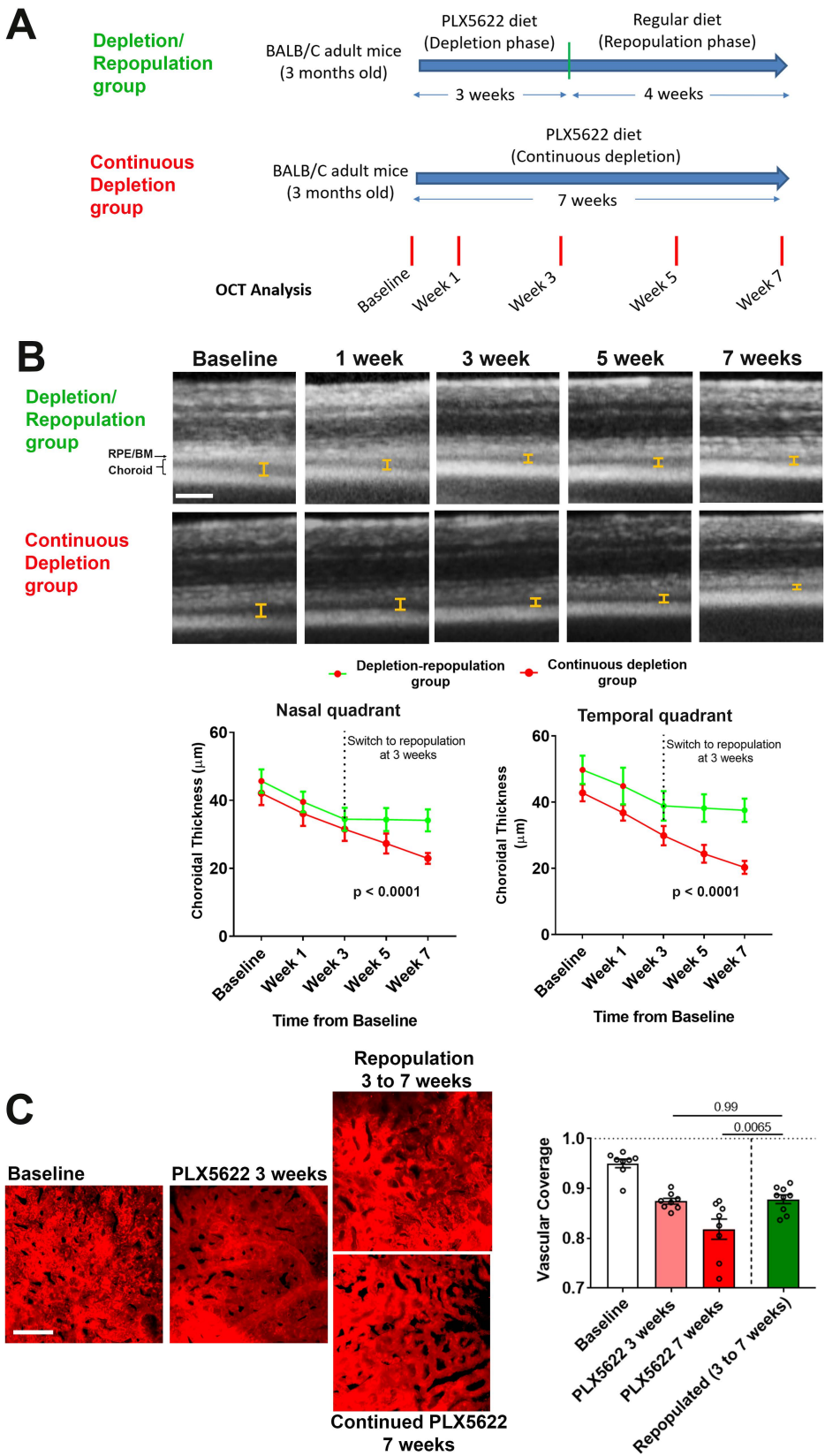
A
Depletion/ Repopulation group
BALB/C adult mice (3 months old)
PLX5622 diet (Depletion phase)
Regular diet (Repopulation phase)
3 weeks
4 weeks
Continuous Depletion group
BALB/C adult mice (3 months old)
PLX5622 diet (Continuous depletion)
7 weeks
OCT Analysis
Baseline
Week 1
Week 3
Week 5
Week 7
B
Baseline
1 week
3 week
5 week
7 weeks
Depletion/ Repopulation group
RPE/BM
Choroid
Continuous Depletion group
Depletion-repopulation group
Continuous depletion group
Nasal quadrant
Switch to repopulation at 3 weeks
Choroidal Thickness (μm)
p < 0.0001
Time from Baseline
Temporal quadrant
Switch to repopulation at 3 weeks
Choroidal Thickness (μm)
p < 0.0001
Time from Baseline
C
Baseline
PLX5622 3 weeks
Repopulation 3 to 7 weeks
Continued PLX5622 7 weeks
0.99
0.0065
Vascular Coverage
Baseline
PLX5622 3 weeks
PLX5622 7 weeks
Repopulated (3 to 7 weeks)

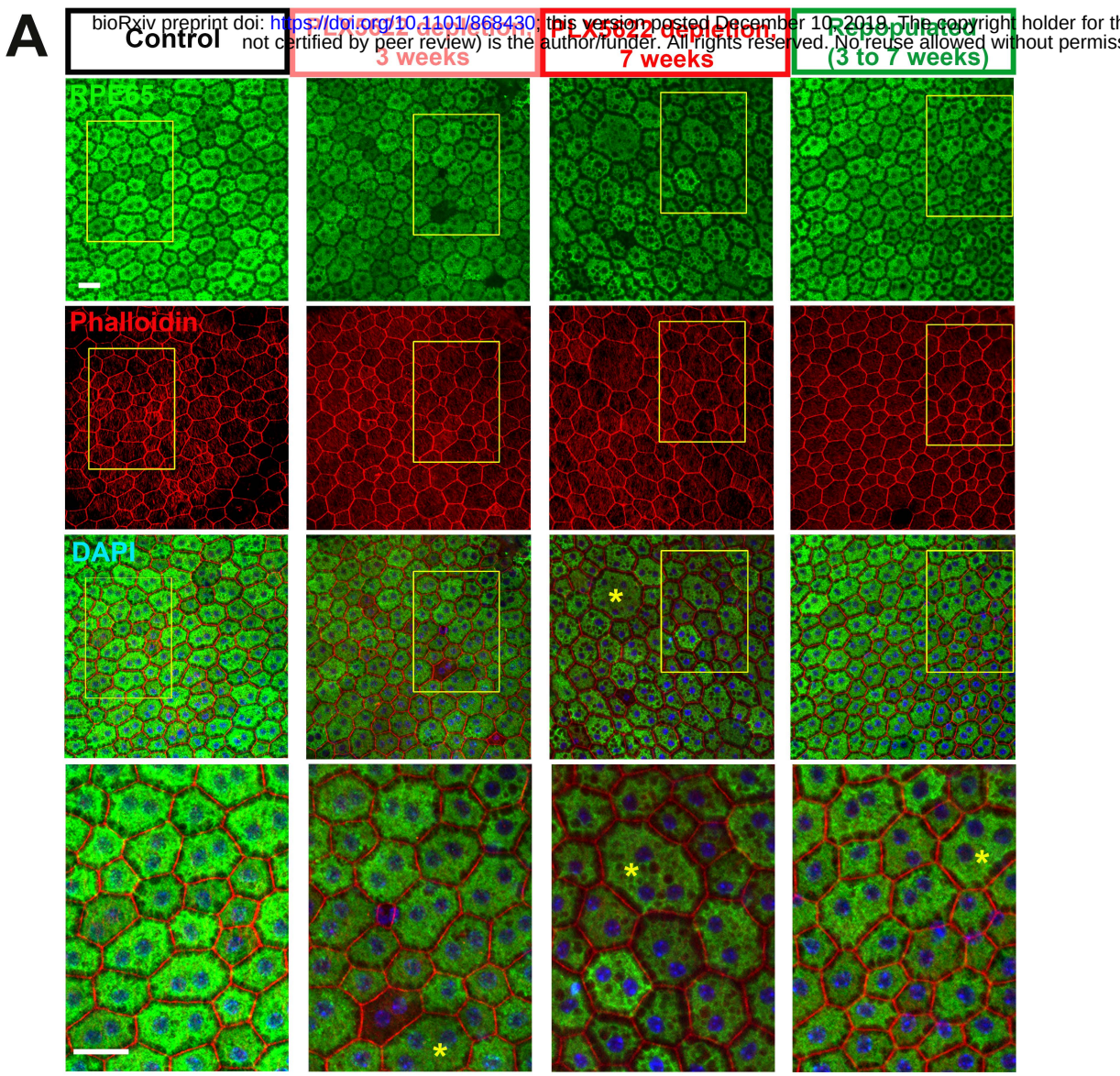

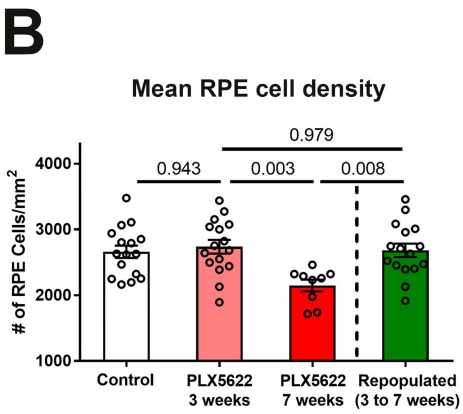

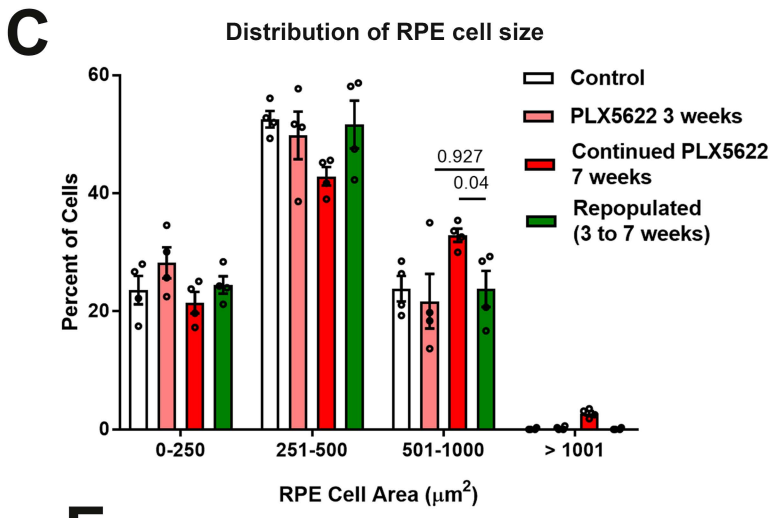

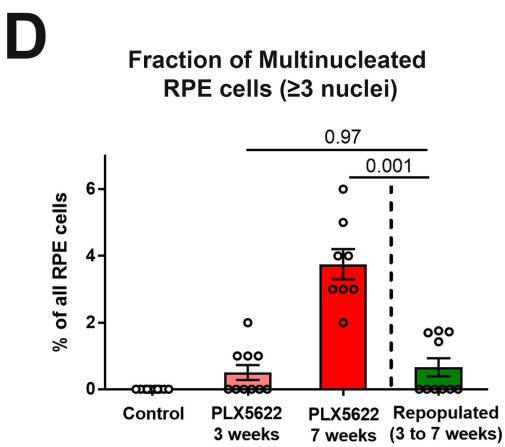

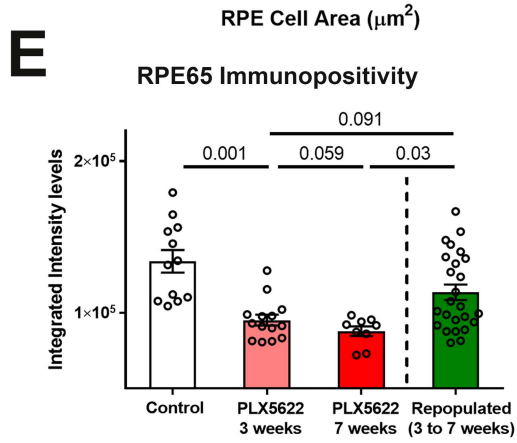

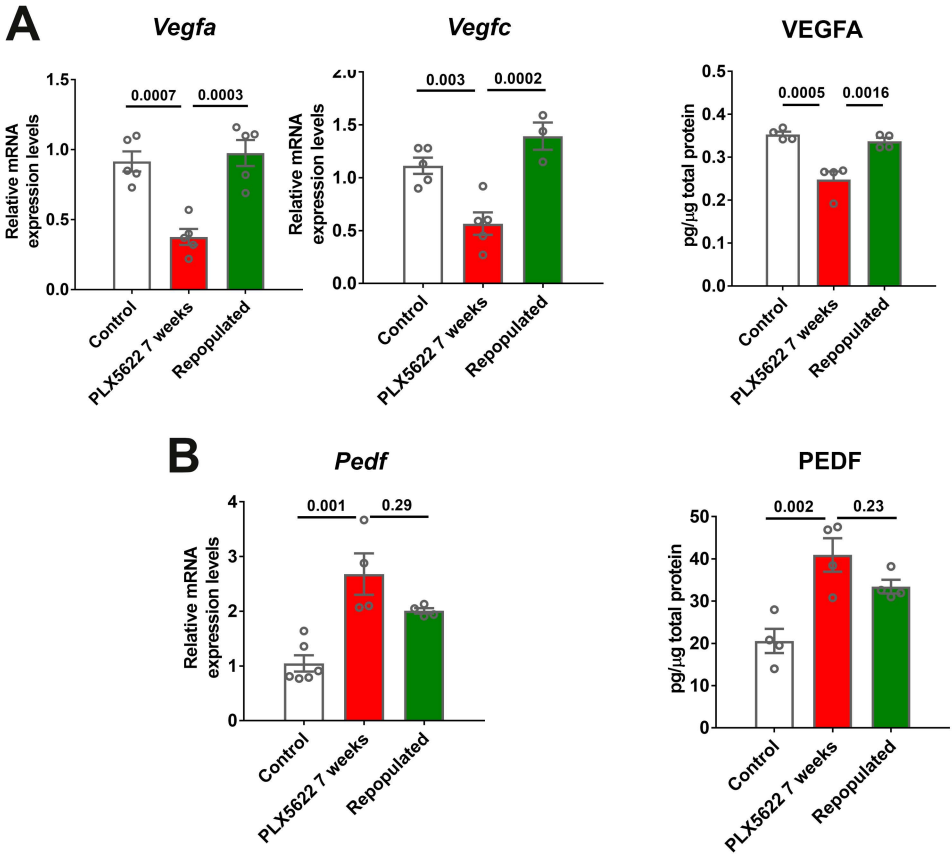
A
Vegfa
Relative mRNA expression levels
0.0007
0.0003
Control
PLX5622 7 weeks
Repopulated
Vegfc
Relative mRNA expression levels
0.003
0.0002
Control
PLX5622 7 weeks
Repopulated
VEGFA
pg/µg total protein
0.0005
0.0016
Control
PLX5622 7 weeks
Repopulated
B
Pedf
Relative mRNA expression levels
0.001
0.29
Control
PLX5622 7 weeks
Repopulated
PEDF
pg/µg total protein
0.002
0.23
Control
PLX5622 7 weeks
Repopulated